EXPERIMENTAL EVALUATION OF FBMC-OQAM CHANNEL ESTIMATION BASED ON MULTIPLE AUXILIARY SYMBOLS

Ronald Nissel[†,‡]*, Sebastian Caban*[†]*, and Markus Rupp*[†]

[†] Technische Universität Wien, Institute of Telecommunications
[‡] Christian Doppler Laboratory for Dependable Wireless Connectivity for the Society in Motion
Gusshausstraße 25, 1040 Vienna, Austria

ABSTRACT

Filter Bank Multi-Carrier (FBMC) has been identified by many authors as a possible successor for orthogonal frequency-division multiplexing in 5G. In this paper, we consider pilot-symbol aided channel estimation in FBMC. To deal with the imaginary interference, inherently caused in FBMC, we employ auxiliary symbols. In contrast to previous works, we propose to use multiple auxiliary symbols per pilot which decreases the peak-to-power average ratio and, for certain operation points, also increases the achievable capacity. The applicability of our channel estimation method is then validated through real world measurements, where we show that multiple auxiliary symbols lead to a higher throughput for practical relevant signal-to-noise ratios.

1. INTRODUCTION

Currently, the wireless communication research community is investigating the next generation of wireless systems (5G) [1–4] and, in particular, which modulation format will succeed Orthogonal Frequency Division Multiplexing (OFDM) [5,6]. FBMC [7–9] has been identified as a strong contender due to its superior spectral properties compared to OFDM [10]. Note that different names, such as cosine-modulated multitone, staggered multitone and OFDM/Offset Quadrature Amplitude Modulation (OQAM), have been used to describe, essentially, the same concept that we will refer to here as FBMC.

Although FBMC behaves in some aspects very similar to OFDM, channel estimation becomes more challenging due to the imaginary interference, inherently caused in FBMC. In principle, we can distinguish between preamble based channel estimation [11, 12] and pilot symbol aided channel estimation [13–16]. We will focus on the latter because pilots allow a simple tracking of the channel in time, which also explains its application in the current LTE standard. In order to straightforwardly employ pilot symbol aided channel estimation in FBMC, we have to cancel the imaginary interference at the pilot positions. To do this, [13] utilized one dedicated symbol per pilot, the so called auxiliary symbol [14]. However, the drawback of this method is a large offset of the auxiliary symbol power compared to the data symbol power. To deal with this problem, we suggested in [16] to use two auxiliary symbols instead of one which improves the Peak-to-Average Power Ratio (PAPR) and increases the achievable capacity for certain Signal-to-Noise Ratio (SNR) ranges. Another method to avoid the power offset, at the expense of computationally complexity, is described in [15] which relies on coding at both, transmitter and receiver. Authors in [17] combined auxiliary symbols and coding, resulting in intermediate complexity and a (small) power offset.

Testbed measurements [18–21] are a crucial step to validate if theoretical concepts work in real word environments. However, due to the underlying complexity of such measurements and the fact that they are quite expensive, measurements are often neglected.

Novel contribution: Firstly, we extend our idea in [16] to a higher number of auxiliary symbols. Secondly, while [16] relies on an oversimplified model based on achievable capacities, we validate our channel estimation method by real world throughput measurements.

2. SYSTEM MODEL

In multicarrier transmissions, the data symbol $x_{l,k}$ at subcarrier position l and time position k is modulated by the basis pulse $g_{l,k}(t)$, so that the transmitted signal $s(t)$, consisting of L subcarriers and K multicarrier symbols, can be written as:

$$s(t) = \sum_{k=0}^{K-1} \sum_{l=0}^{L-1} g_{l,k}(t)\, x_{l,k}, \tag{1}$$

with

$$g_{l,k}(t) = p(t - kT)\, \mathrm{e}^{\mathrm{j}2\pi\, lF\,(t-kT)}\, \mathrm{e}^{\mathrm{j}\theta_{l,k}}. \tag{2}$$

The basis pulse in (2) is essentially a time and frequency shifted version of the prototype filter $p(t)$. In order to maximize the throughput, time spacing T together with frequency spacing F should be as small as possible. However, orthogonality requires $TF \geq 1$. Besides orthogonality and $TF = 1$, another desired property is localization of the pulse in both, time and frequency. Unfortunately, not all of these properties can be fulfilled at the same time according to the Balian-Low theorem [22]. In OFDM ($\theta_{l,k} = 0$), the prototype filter $p(t)$ is based on a rectangular function, violating the requirement of frequency localization (and $TF > 1$ if a Cyclic Prefix (CP) is used). In FBMC, on the other hand, the (complex) orthogonality condition is replaced by the less strict real orthogonality condition. For our FBMC system we consider a basis pulse which is based on Hermite polynomials $H_i(\cdot)$, as suggested in [23], because it offers a good trade-off between time localization and frequency localization and the pulse has the same shape in the time domain and in the frequency domain, allowing us to exploit symmetries. Such pulse, see [16], guarantees orthogonality of (2) for a time spacing of $T = T_0$ and a frequency spacing of $F = \frac{2}{T_0}$. The idea in FBMC is now to reduce the time-spacing as well as the frequency spacing by a factor of two, leading to $TF = \frac{1}{2}$ (real symbols) which is equivalent (in terms of transmitted information per time unit) to $TF = 1$ (complex

This work has been funded by the Christian Doppler Laboratory for Wireless Technologies for Sustainable Mobility. The financial support by the Austrian Federal Ministry of Science, Research and Economy, the National Foundation for Research, Technology and Development, and the TU Wien is gratefully acknowledged.

symbols). Of course, such time-frequency squeezing causes interference which, however, is shifted to the purely imaginary domain by $\theta_{l,k} = \frac{\pi}{2}(l+k)$ in (2), making such system very similar to OFDM. At the receiver, we obtain the received symbol $y_{l,k}$ by projecting the received signal $r(t)$ onto the basis pulse $g_{l,k}(t)$, leading to:

$$y_{l,k} = \langle r(t), g_{l,k}(t) \rangle = \int_{-\infty}^{-\infty} r(t) g_{l,k}^*(t)\, \mathrm{d}t, \tag{3}$$

with $\langle \cdot, \cdot \rangle$ denoting the inner product. In OFDM, the complex orthogonality condition guarantees that $\langle g_{l_1,k_1}(t), g_{l_2,k_2}(t) \rangle = \delta_{(l_1-l_2),(k_1-k_2)}$ while in FBMC we observe imaginary interference which has to be canceled by taking the real part, that is, $\Re\{\langle g_{l_1,k_1}(t), g_{l_2,k_2}(t) \rangle\} = \delta_{(l_1-l_2),(k_1-k_2)}$. In order to simplify analytical investigations, we stack the transmitted data symbols $x_{l,k}$ in a vector $\mathbf{x}$, the receiced data symbols $y_{l,k}$ in a vector $\mathbf{y}$ and the channel coefficients $h_{l,k}$ in a vector $\mathbf{h}$ according to:

$$\mathbf{x} = \begin{bmatrix} x_{1,1} & x_{2,1} & \cdots & x_{L,1} & x_{1,2} & \cdots & x_{L,K} \end{bmatrix}^{\mathrm{T}} \tag{4}$$

$$\mathbf{y} = \begin{bmatrix} y_{1,1} & y_{2,1} & \cdots & y_{L,1} & y_{1,2} & \cdots & y_{L,K} \end{bmatrix}^{\mathrm{T}} \tag{5}$$

$$\mathbf{h} = \begin{bmatrix} h_{1,1} & h_{2,1} & \cdots & h_{L,1} & h_{1,2} & \cdots & h_{L,K} \end{bmatrix}^{\mathrm{T}}. \tag{6}$$

We assume Additive White Gaussian Noise (AWGN) and a channel for which the Doppler spread and the delay spread are assumed to be so low, that inter-carrier interference and inter-symbol interference can be neglected. We can then write our transmission system model in matrix notation as [24]:

$$\mathbf{y} = \mathrm{diag}(\mathbf{h})\mathbf{D}\mathbf{x} + \mathbf{n}, \tag{7}$$

where the element in the $(l_1 + k_1 L)$-th column and the $(l_2 + k_2 L)$-th row of $\mathbf{D}$ is given by:

$$[\mathbf{D}]_{(l_1+k_1 L),(l_2+k_2 L)} = \langle g_{l_2,k_2}(t), g_{l_1,k_1}(t) \rangle. \tag{8}$$

In OFDM, matrix $\mathbf{D}$ becomes an identity matrix, $\mathbf{D} = \mathbf{I}_{LK}$, whereas for FBMC, matrix $\mathbf{D}$ has imaginary elements at the off-diagonal and only by taking the real part we observe an identity matrix, $\Re\{\mathbf{D}\} = \mathbf{I}_{LK}$. Vector $\mathbf{n}$ in (7) represents Gaussian distributed noise $\mathbf{n} \sim \mathcal{CN}(0, P_{\mathrm{n}}\,\mathbf{D})$. So far, we assumed that OFDM uses a time-frequency spacing of $TF = 1$. However, in practice, a CP is usually included, sacrificing spectral efficiency ($TF > 1$) in order to increase robustness. Note that the cyclic prefix extends the rectangular pulse at the transmitter by the length of the CP, so that the condition of orthogonality transforms to bi-orthogonality.

3. PILOT-SYMBOL AIDED CHANNEL ESTIMATION

The idea of pilot-symbol aided channel estimation [24, 25] is quite simple: dedicated "data symbols", the so called pilots, are known a priory at the receiver. At the pilot positions $(l,k) \in \mathcal{P}$, we divide the received symbols $y_{l,k}$ by the pilot symbols $x_{l,k}$, which delivers a Least Squares (LS) estimation of the channel $h_{l,k}$ and can be interpreted as sampling of the channel transfer function at the pilot positions. In vector notation this reads as:

$$\hat{\mathbf{h}}_{\mathcal{P}}^{\mathrm{LS}} = \mathrm{diag}(\mathbf{x}_{\mathcal{P}})^{-1} \mathbf{y}_{\mathcal{P}}, \tag{9}$$

where $\mathbf{x}_{\mathcal{P}}$ represents all pilot symbols in vectorized form and $\mathbf{y}_{\mathcal{P}}$ the received data symbols at the pilot positions. In order to obtain the remaining channel coefficients, that is, the channel at the data positions $(l,k) \in \mathcal{D}$, we interpolate and extrapolate:

$$\hat{\mathbf{h}} = \mathbf{A}\hat{\mathbf{h}}_{\mathcal{P}}^{\mathrm{LS}}. \tag{10}$$

Here, $\mathbf{A} \in \mathbb{C}^{LK \times |\mathcal{P}|}$ describes a large range of possible interpolation methods, such as, linear, spline, nearest neighbor or Minimum Mean Squared Error (MMSE) interpolation. In OFDM, the channel estimation works exactly as described above, but in FBMC it becomes more challenging due to the imaginary interference. FBMC

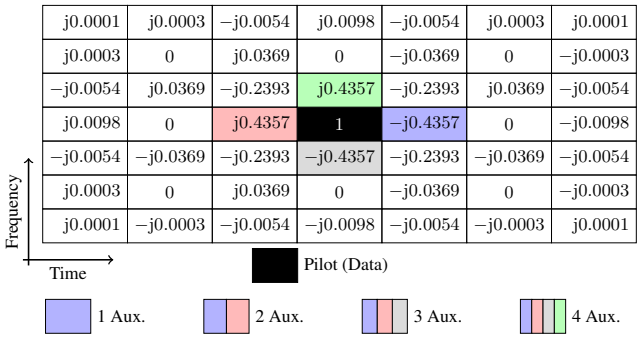

Fig. 1. In FBMC, neighboring symbols cause imaginary interference, whereby the corresponding interference weights are shown. Auxiliary symbols allow to cancel the imaginary interference, so that pilot symbol aided channel estimation can be straightforwardly applied. A higher number of auxiliary symbols decreases the harmful power offset, as shown in Table 1.

Table 1. Auxiliary symbol power offset ($\alpha = 0.4357$)

	1 Aux.	2 Aux.	3 Aux.	4 Aux.
$\frac{P_{\mathcal{A}}}{P_{\mathcal{D}}}$	$\frac{1-\alpha^2}{\alpha^2} = 4.27$	$\frac{1-2\alpha^2}{(2\alpha)^2} = 0.82$	$\frac{1-3\alpha^2}{(3\alpha)^2} = 0.25$	$\frac{1-4\alpha^2}{(4\alpha)^2} = 0.08$

is based on the idea of taking the real part in order to get rid of the imaginary interference. However, this only works after channel equalization which is clearly not possible prior to channel estimation. Thus, the channel estimation has to be performed in the complex domain but the random imaginary interference has the same power as the data symbols, leading to a signal-to-interference ratio of 0 dB, which is clearly too low for accurate channel estimations. In order to straightforwardly employ pilot symbol aided channel estimation, we thus have to cancel the imaginary interference at the pilot positions which will be accomplished in this paper by auxiliary pilot symbols [14].

4. AUXILIARY PILOT SYMBOLS

As indicated in (7) and shown in Figure 1, several symbols close to the pilot symbol cause imaginary interference. In the classical approach [13], one of these symbols is utilized to cancel the imaginary interference from all other symbols. However, the imaginary interference weight is smaller than one, in our case $0.4357 < 1$, which implies that the auxiliary symbol power has to be increased in order to compensate for this loss. Let us take a closer look at this power offset: the auxiliary symbol has to compensate the imaginary interference from the surounding symbols (excluding the auxiliary symbol), leading to a interference power of $(1 - 0.4357^2)$. Additionally, the auxiliary symbol has to be multiplied by $\frac{1}{0.4357}$ to compensate for the loss given by the interference weight. Thus, the auxiliary symbol power is $\frac{(1-0.4357^2)}{0.4357^2} = 4.27$ times higher than the data symbol power. In [16] we suggested to use two auxiliary symbols which split the cancellation job between them, decreasing the power offset from 4.27 to 0.82. By extending this method to three and four auxiliary symbols, we can further decrease the power offset, as shown in Table 1. Of course, an increased number of auxiliary symbols per pilot also decreases the number of available data symbols. However, as we will show in Section 5, the saved power offsets the loss of data symbols, leading to an increased throughput for certain SNR ranges. The general condition for auxiliary symbols can

be expressed as [16]:

$$\mathbf{x}_{\mathcal{A}} = \mathbf{D}^{\#}_{\mathcal{P},\mathcal{A}} \left(\mathbf{I}_{\mathcal{P}} - \mathbf{D}_{\mathcal{P},\mathcal{P}} \right) \mathbf{x}_{\mathcal{P}} - \mathbf{D}^{\#}_{\mathcal{P},\mathcal{A}} \mathbf{D}_{\mathcal{P},\mathcal{D}} \mathbf{x}_{\mathcal{D}}, \quad (11)$$

with

$$\mathbf{D}^{\#}_{\mathcal{P},\mathcal{A}} = \mathbf{D}^{H}_{\mathcal{P},\mathcal{A}} \left(\mathbf{D}_{\mathcal{P},\mathcal{A}} \mathbf{D}^{H}_{\mathcal{P},\mathcal{A}} \right)^{-1}. \quad (12)$$

The vector $\mathbf{x}_{\mathcal{P}} \in \mathbb{R}^{|\mathcal{P}|\times 1}$ denotes all those elements of $\mathbf{x}$ at the pilot positions. The same applies to $\mathbf{x}_{\mathcal{D}} \in \mathbb{R}^{|\mathcal{D}|\times 1}$ at the data positions and $\mathbf{x}_{\mathcal{A}} \in \mathbb{R}^{|\mathcal{A}|\times 1}$ at the auxiliary positions. Similar, matrix $\mathbf{D}_{\mathcal{P},\mathcal{D}} \in \mathbb{C}^{|\mathcal{P}|\times|\mathcal{D}|}$ consists of the row elements and the column elements of $\mathbf{D}$ at the pilot positions respectively data positions. Again, the same is true for $\mathbf{D}_{\mathcal{P},\mathcal{P}}$ and $\mathbf{D}_{\mathcal{P},\mathcal{A}}$.

Let us denote the data symbol power by $P_{\mathcal{D}} = \mathbb{E}\{|x_{l,k}|^2\}$ for $(l,k) \in \mathcal{D}$, the pilot symbol power by $P_{\mathcal{P}} = \mathbb{E}\{|x_{l,k}|^2\}$ for $(l,k) \in \mathcal{P}$ and the (average) auxiliary symbol power by $P_{\mathcal{A}} = \frac{1}{|\mathcal{A}|} \operatorname{tr}\{\mathbb{E}\{\mathbf{x}_{\mathcal{A}} \mathbf{x}^{H}_{\mathcal{A}}\}\}$ with $\mathbf{x}_{\mathcal{A}}$ given by (11). By ignoring edge effects and if the pilots are spaced sufficiently far away from each other so that no noticeable interference occurs between them, $P_{\mathcal{A}}$ is given in Table 1. The SNR can be expressed as:

$$\mathrm{SNR}_{\mathrm{OFDM}} = \frac{|\mathcal{D}_{\mathrm{OFDM}}|\ P_{\mathcal{D},\mathrm{OFDM}} + |\mathcal{P}_{\mathrm{OFDM}}|\ P_{\mathcal{P},\mathrm{OFDM}}}{L_{\mathrm{OFDM}}\, K_{\mathrm{OFDM}}\, P_{\mathrm{n}}} \quad (13)$$

$$\mathrm{SNR}_{\mathrm{FBMC}} = \frac{|\mathcal{D}_{\mathrm{FnA.}}|\ P_{\mathcal{D},\mathrm{FnA.}} + |\mathcal{P}_{\mathrm{FnA.}}|\ P_{\mathcal{P},\mathrm{FnA.}} + |\mathcal{A}_{\mathrm{FnA.}}|\ P_{\mathcal{A},\mathrm{FnA.}}}{L_{\mathrm{FBMC}}\, K_{\mathrm{FBMC}}\, \frac{P_{\mathrm{n}}}{2}}, \quad (14)$$

where the subscript "FnA." is short for FBMC employing n=1 . . . 4 auxiliary symbols per pilot. In FBMC, we operate in the real domain, so that the complex noise power is reduced by a factor of two, as shown in (14). For a fair comparison of OFDM and FBMC, we always consider the same average transmit power P_{S}, defined as:

$$P_{\mathrm{S}} = \frac{1}{KT} \int_{-\infty}^{-\infty} \mathbb{E}\{|s(t)|^2\}\, \mathrm{d}t, \quad (15)$$

where KT represents the length of the signal in the time domain and $s(t)$ the transmitted signal given in (1). Let us assume that OFDM and FBMC both use the same frequency spacing F. For the same transmit power P_{S}, the following relationship holds:

$$\mathrm{SNR}_{\mathrm{FBMC}} = \mathrm{SNR}_{\mathrm{OFDM}} \frac{L^{\mathrm{OFDM}}}{L^{\mathrm{FBMC}}}. \quad (16)$$

In particular, for the same number of subcarriers L, both have the same SNR although FBMC experiences only half the noise power as shown in (14). However, because the pulses overlap in time, the symbol power also has to be reduced by a factor of two, leading to the same SNR. If FBMC employs a higher number of subcarriers, the transmit power has to be distributed over a higher bandwidth which reduces the available power of each symbol while at the same time the noise power remains constant, therefore reducing the SNR.

Now that we have specified the available data symbol power, see (13), (14) and (15), let us investigate the achievable capacities (which include the system overheads such as pilot symbols). We interpret each time-frequency position as a separate Rayleigh fading channel, so that the achievable ergodic capacities for perfect channel knowledge become [26]:

$$C_{\mathrm{OFDM}} = \frac{|\mathcal{D}_{\mathrm{OFDM}}|\ \mathbb{E}_h\left\{ \log_2\left(1 + |h|^2 \frac{P_{\mathcal{D},\mathrm{OFDM}}}{P_{\mathrm{n}}}\right)\right\}}{K_{\mathrm{OFDM}}\, T_{\mathrm{OFDM}}} \quad (17)$$

$$C_{\mathrm{FBMC,n\text{-}Aux.}} = \frac{|\mathcal{D}_{\mathrm{FnA.}}|\ \mathbb{E}_h\left\{ \frac{1}{2}\log_2\left(1 + |h|^2 \frac{P_{\mathcal{D},\mathrm{FnA.}}}{P_{\mathrm{n}}/2}\right)\right\}}{K_{\mathrm{FBMC}}\, T_{\mathrm{FBMC}}}, \quad (18)$$

where h reflects the unit power Rayleigh fading channel, $h \sim$ Rayleigh(1). The main idea of this paper is to increase the number of auxiliary symbols $|\mathcal{A}|$ which reduces the number of data symbols $|\mathcal{D}|$, but increases the available power for the remaining data symbols because the power of auxiliary symbols can be greatly reduced, see Table 1.

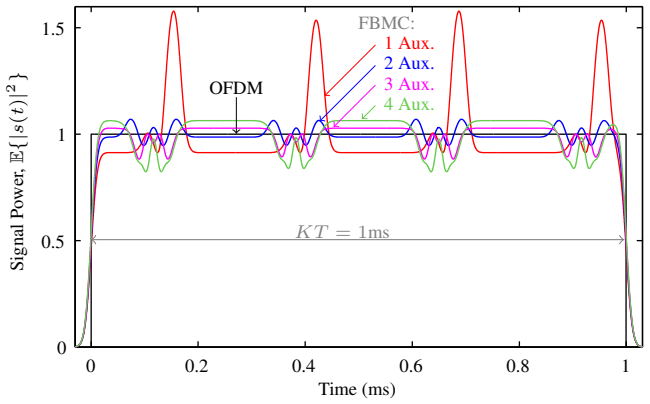

Fig. 2. For a fair comparison of different modulation schemes, we always consider the same transmit power, here $P_{\mathrm{S}} = 1$. One auxiliary symbol per pilot causes large peaks in the signal power at auxiliary symbol position, which also lead so a large PAPR. These harmful effects can be mitigated by increasing the number of auxiliary symbols per pilot.

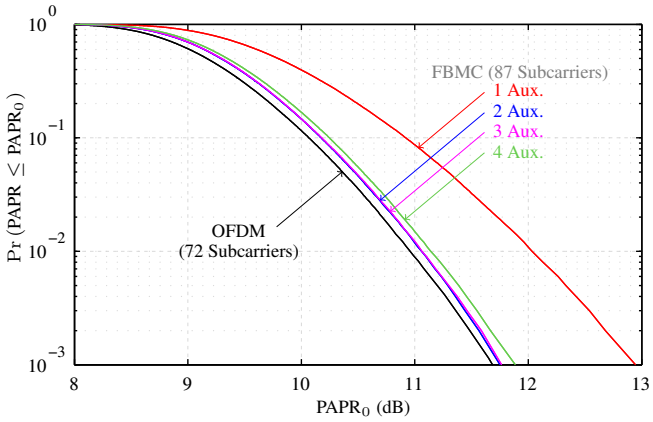

Fig. 3. The large power offset of one auxiliary symbol per pilot leads to a poor PAPR. By using multiple auxiliary symbols per pilot, we can mitigate this harmful effect. Because FBMC employs a higher number of subcarriers compared to OFDM, its PAPR is also (marginally) worse.

5. TESTBED MEASUREMENTS

FBMC has a higher spectral efficiency than OFDM because it does not employ a CP and, due to much lower side lobes, requires a smaller guard band. In order to validate this improvement and to show the feasibility of our channel estimation method, we measure an 1.4 MHz LTE like system using the Vienna Wireless Testbed [27–30]. For OFDM, we assume a subcarrier spacing of $F = 15\,\mathrm{kHz}$, $K = 14$ symbols and a CP length of 4.76 µs, resulting in a transmission time of $KT = 1\,\mathrm{ms}$. FBMC also employs a subcarrier spacing of $F = 15\,\mathrm{kHz}$ and uses $K = 30$ (real symbols), also leading to a transmission time of $KT = 1\,\mathrm{ms}$. Although LTE occupies 1.4 MHz, it only utilizes $L = 72$ subcarriers ($LF = 1.08\,\mathrm{MHz}$). Due to much lower side lobes in FBMC, we are able to increase the number of

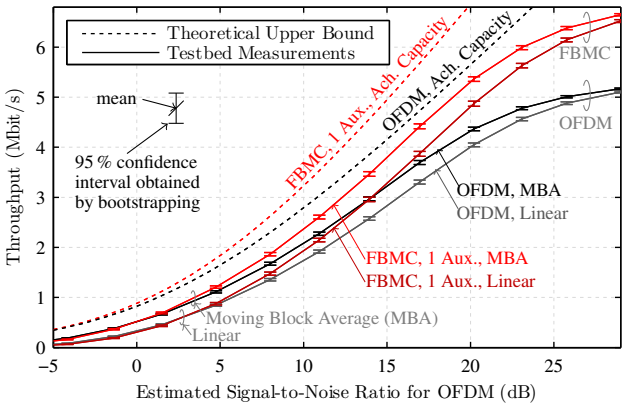

Fig. 4. FBMC outperforms OFDM because it uses the available bandwidth more efficiently and does not employ a CP. Because the channel is highly correlated, moving block average performs better than linear interpolation. Compared to the theoretical upper bound, the throughput is approximately 3 dB off (ignoring saturation for high SNR values).

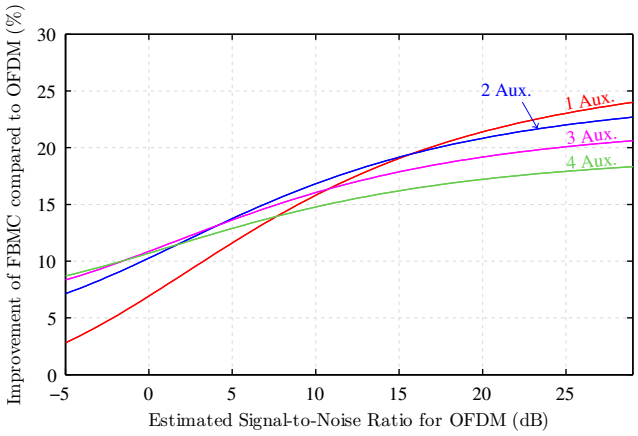

Fig. 5. Achievable capacities, see (17) and (18): Relative improvement of FBMC compared to OFDM. Depending on the SNR, it is possible to improve the performance of one auxiliary symbol by employing multiple auxiliary symbols.

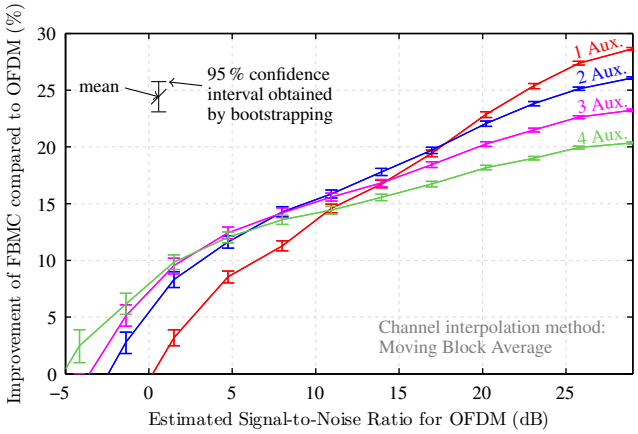

Fig. 6. Measured throughput: Improvement of FBMC compared to OFDM for channel interpolation based on moving block average. Overall, the possible improvement behaves similar to our theoretical considerations in Figure 5. However, for a high SNR and a low SNR, we observe deviations due to the limited number of CQI values.

subcarriers to $L = 87$, corresponding to $LF = 1.305\,\text{MHz}$ and a power spectral density that is below 84 dB of its maximum value for frequencies outside the 1.4 MHz bandwidth. For OFDM, the pilot symbol pattern is chosen according to the LTE standard, that is, a diamond-shaped pattern with a pilot density of $|\mathcal{P}|/(KT\,LF) = 0.044$. The pilot symbol power is the same as the data symbol power, $P_{\mathcal{P}} = P_{\mathcal{D}}$. For FBMC, we chose a similar pilot pattern where, in particular, the pilot density is the same as in OFDM. However, the pilot power is increased by a factor of two, $P_{\mathcal{P}} = 2P_{\mathcal{D}}$, so that the channel estimation (complex domain) and the data transmission (real domain) experience the same SNR. We transmit our signal at a carrier frequency of 2.4955 GHz and obtain different channel realizations, corresponding to Rayleigh fading, by moving (and rotating) the receive antenna to 4096 different positions within a 4×4 wavelength grid. For the measured throughput, we use turbo coding in combination with 15 Channel Quality Indicator (CQI) values, corresponding to a specific modulation order and code rate, as defined in the LTE standard. We transmit the signal for all CQI values consecutively and choose at the receiver the highest possible throughput, that is, the highest CQI value for which all data bits were detected correctly after turbo decoding.

Figure 2 compares the expected transmit power for OFDM and FBMC. The large power offset of one auxiliary symbol also leads to a high PAPR (the peak values are considered over the whole 1 ms time interval), as shown in Figure 3. By using our approach of multiple auxiliary symbols, we can mitigate these harmful effects.

The measured throughput and the theoretical upper bound, see (17) and (18), are shown in Figure 4. To keep the illustration simple, we considered only the case of one auxiliary symbol here. Instead we compare different interpolation methods, see (10), namely, linear interpolation (of the three closest pilot estimates) and moving block average, which averages all pilot estimates who are within a time-frequency range of 15 time-symbols and 12 subcarriers. The latter is possible because the channel is highly correlated in both, time and frequency, so that moving block average outperforms linear interpolation by approximately 1.7 dB SNR.

Using the SNR relationships given in (14) and (16), we calculated that for one auxiliary symbol, the data symbol SNR is shifted by 1.22 dB compared to OFDM. Similar, for two auxiliary symbols it is 0.88 dB, for three 0.7 dB and for four 0.55 dB. Thus, by increasing the number of auxiliary symbols, we increase the data symbol SNR, but at the same time, the number of data symbols decreases. The overall effect on the achievable capacity is shown in Figure 5 and for the measured throughput in Figure 6. For a low SNR, the throughput-gain of an increased data symbol SNR outweighs the throughput-loss due to fewer data symbols, so that multiple auxiliary symbols per pilot perform better than one auxiliary symbol. For a high SNR, we observe an opposite effect. We also see that there is little advantage of using more than two auxiliary symbols.

6. CONCLUSION

One auxiliary symbol per pilot, as usually considered in literature, leads to a poor PAPR, so that we suggest to use multiple auxiliary symbols. For practical relevant SNR ranges, multiple auxiliary symbols even increase the throughput. By measuring the throughput using the Vienna Wireless Testbed, we show that our approach of multiple auxiliary symbols works in real world scenarios.

7. REFERENCES

[1] J. G. Andrews, S. Buzzi, W. Choi, S. V. Hanly, A. Lozano, A. C. Soong, and J. C. Zhang, "What will 5G be?" *IEEE Journal on Selected Areas in Communications*, vol. 32, no. 6, pp. 1065–1082, 2014.

[2] S. Schwarz and M. Rupp, "Society in motion: Challenges for LTE and beyond mobile communications," *IEEE Commun. Mag., Feature Topic: LTE Evolution*, vol. 54, no. 5, 2016.

[3] R. Nissel and M. Rupp, "Dynamic spectrum allocation in cognitive radio: Throughput calculations," in *IEEE International Black Sea Conference on Communications and Networking (BlackSeaCom)*, Varna, Bulgaria, Jun. 2016.

[4] E. Zöchmann, S. Schwarz, and M. Rupp, "Comparing antenna selection and hybrid precoding for millimeter wave wireless communications," in *IEEE Sensor Array and Multichannel Signal Processing Workshop (SAM)*, Rio de Janeiro, Brazil, Jul. 2016.

[5] G. Wunder, P. Jung, M. Kasparick, T. Wild, F. Schaich, Y. Chen, S. Brink, I. Gaspar, N. Michailow, A. Festag *et al.*, "5GNOW: non-orthogonal, asynchronous waveforms for future mobile applications," *IEEE Communications Magazine*, vol. 52, no. 2, pp. 97–105, 2014.

[6] P. Banelli, S. Buzzi, G. Colavolpe, A. Modenini, F. Rusek, and A. Ugolini, "Modulation formats and waveforms for 5G networks: Who will be the heir of OFDM?: An overview of alternative modulation schemes for improved spectral efficiency," *IEEE Signal Process. Mag.*, vol. 31, no. 6, pp. 80–93, 2014.

[7] H. Bölcskei, "Orthogonal frequency division multiplexing based on offset QAM," in *Advances in Gabor analysis*. Springer, 2003, pp. 321–352.

[8] B. Farhang-Boroujeny and C. H. Yuen, "Cosine modulated and offset QAM filter bank multicarrier techniques: a continuous-time prospect," *EURASIP Journal on Advances in Signal Processing*, vol. 2010, p. 6, 2010.

[9] M. Bellanger, D. Le Ruyet, D. Roviras, M. Terré, J. Nossek, L. Baltar, Q. Bai, D. Waldhauser, M. Renfors, T. Ihalainen *et al.*, "FBMC physical layer: a primer," *PHYDYAS*, 2010.

[10] B. Farhang-Boroujeny, "OFDM versus filter bank multicarrier," *IEEE Signal Processing Magazine*, vol. 28, no. 3, pp. 92–112, 2011.

[11] D. Katselis, E. Kofidis, A. Rontogiannis, and S. Theodoridis, "Preamble-based channel estimation for CP-OFDM and OFDM/OQAM systems: A comparative study," *IEEE Trans. Signal Process.*, vol. 58, no. 5, pp. 2911–2916, 2010.

[12] E. Kofidis, D. Katselis, A. Rontogiannis, and S. Theodoridis, "Preamble-based channel estimation in OFDM/OQAM systems: a review," *Signal Processing*, vol. 93, no. 7, pp. 2038–2054, 2013.

[13] J.-P. Javaudin, D. Lacroix, and A. Rouxel, "Pilot-aided channel estimation for OFDM/OQAM," in *IEEE Vehicular Technology Conference (VTC)*, vol. 3, 2003, pp. 1581–1585.

[14] T. H. Stitz, T. Ihalainen, A. Viholainen, and M. Renfors, "Pilot-based synchronization and equalization in filter bank multicarrier communications," *EURASIP Journal on Advances in Signal Processing*, vol. 2010, p. 9, 2010.

[15] C. Lélé, R. Legouable, and P. Siohan, "Channel estimation with scattered pilots in OFDM/OQAM," in *IEEE Workshop on Signal Processing Advances in Wireless Communications (SPAWC)*, 2008, pp. 286–290.

[16] R. Nissel and M. Rupp, "On pilot-symbol aided channel estimation in FBMC-OQAM," in *IEEE International Conference on Acoustics, Speech and Signal Processing (ICASSP)*, Shanghai, China, March 2016.

[17] W. Cui, D. Qu, T. Jiang, and B. Farhang-Boroujeny, "Coded auxiliary pilots for channel estimation in FBMC-OQAM systems," *IEEE Transactions on Vehicular Technology*, vol. 65, no. 5, pp. 2936–2946, May 2016.

[18] R. Nissel and M. Rupp, "Doubly-selective MMSE channel estimation and ICI mitigation for OFDM systems," in *IEEE International Conference on Communications (ICC)*, London, UK, June 2015.

[19] R. Nissel, M. Lerch, and M. Rupp, "Experimental validation of the OFDM bit error probability for a moving receive antenna," in *IEEE Vehicular Technology Conference (VTC)*, Vancouver, Canada, Sept 2014.

[20] R. Nissel, S. Caban, and M. Rupp, "Closed-Form capacity expression for low complexity BICM with uniform inputs," in *IEEE International Symposium on Personal, Indoor and Mobile Radio Communications (PIMRC)*, Hong Kong, P.R. China, Aug. 2015.

[21] E. Zöchmann, M. Lerch, S. Caban, R. Langwieser, C. F. Mecklenbräuker, and M. Rupp, "Directional evaluation of receive power, Rician K-factor and RMS delay spread obtained from power measurements of 60GHz indoor channels," in *IEEE-APS Topical Conference on Antennas and Propagation in Wireless Communications (APWC)*, Cairns, Australia, Sep. 2016.

[22] H. G. Feichtinger and T. Strohmer, *Gabor analysis and algorithms: Theory and applications*. Springer Science & Business Media, 2012.

[23] R. Haas and J.-C. Belfiore, "A time-frequency well-localized pulse for multiple carrier transmission," *Wireless Personal Communications*, vol. 5, no. 1, pp. 1–18, 1997.

[24] R. Nissel and M. Rupp, "Bit error probability for pilot-symbol aided channel estimation in FBMC-OQAM," in *IEEE International Conference on Communications (ICC)*, Kuala Lumpur, Malaysia, May 2016.

[25] R. Nissel, M. Lerch, M. Šimko, and M. Rupp, "Bit error probability for pilot-symbol-aided OFDM channel estimation in doubly-selective channels," in *International ITG Workshop on Smart Antennas (WSA)*, Erlangen, Germany, Mar 2014.

[26] T. M. Cover and J. A. Thomas, *Elements of information theory*. John Wiley & Sons, 2012.

[27] M. Lerch, S. Caban, M. Mayer, and M. Rupp, "The Vienna MIMO testbed: Evaluation of future mobile communication techniques." *Intel Technology Journal*, vol. 4, pp. 58–69, 2014.

[28] M. Lerch, "Experimental comparison of fast-fading channel interpolation methods for the LTE uplink," in *International Symposium ELMAR*, Zadar, Croatia, Sep. 2015.

[29] M. Lerch, S. Caban, E. Zöchmann, and M. Rupp, "Quantifying the repeatability of wireless channels by quantized channel state information," in *IEEE Sensor Array and Multichannel Signal Processing Workshop (SAM)*, Rio de Janeiro, Brazil, Jul. 2016.

[30] E. Zöchmann, S. Caban, M. Lerch, and M. Rupp, "Resolving the angular profile of 60 GHz wireless channels by Delay-Doppler measurements," in *IEEE Sensor Array and Multichannel Signal Processing Workshop (SAM)*, Rio de Janeiro, Brazil, Jul. 2016.